A Method for Estimating Rain Rate and Drop Size Distribution from Polarimetric Radar Measurements

Guifu Zhang, J. Vivekanandan, and Edward Brandes

***Abstract*—Polarimetric radar measurements are sensitive to the size, shape and orientation of raindrops and provide information about drop size distribution (DSD), canting angle distribution and rain rate. In this paper, we propose and demonstrate a method for retrieving DSD parameters for calculating rain rate and the characteristic particle size. The DSD is assumed to be a Gamma distribution and the governing parameters are retrieved from radar measurements: reflectivity (Z_{HH}), differential reflectivity (Z_{DR}), and a constrained relation between the shape (μ) and slope (Λ) parameters derived from video disdrometer observations. The estimated rain rate is compared with that obtained from more traditional methods and the calculated characteristic size is compared with the measured values. The calculated K_{DP} based on the retrieved Gamma DSD is also compared with measurements. The proposed method shows improvement over the existing models and techniques because it can retrieve all three parameters of the Gamma distribution. For maintaining the continuity of earlier published results, raindrop shape is assumed to be equilibrium.**

I. Introduction

SINCE a differential reflectivity was first proposed for rain estimation by Seliga and Bringi in 1976 [1], the polarimetric radar technique has attracted attention in radar meteorology [2]–[4]. Much progress has been made in retrieving cloud microphysical properties and rain rate [5], [6]. Polarization parameters such as radar reflectivity (Z_{HH}), differential reflectivity (Z_{DR}), linear reflectivity difference (Z_{DP}), specific differential phase shift (K_{DP}), linear depolarization ratio (LDR), as well as the correlation coefficient (ρ_{HV}) have been successfully measured. These polarimetric measurements provide more information about precipitation and allow better characterization of hydrometeors. In general, Z_{HH}, Z_{DR}, and K_{DP} are used to estimate rain rate and drop spectrum, since they depend mainly on drop size and shape [7]–[12]. LDR and the covariances are used for retrieving canting angles because they are sensitive to particle orientation [13], [14].

Rain rate (R) estimation from radar measurements is based on empirical models such as Z–R, $R(Z, Z_{DR})$, and $R(K_{DP})$ relations, which are usually derived from regression analysis of radar and rain gauge measurements or numerical simulations [7], [8], [15]. Fixed empirical relations cannot give accurate estimation results for various types of rain. The instantanous reflectivity-based rain rate estimate is affected by various factors such as the shape and size distribution of raindrops. The Z–R relation can have a factor of two error for rain estimation since Z_{HH} is the sixth moment of the drop spectrum, while rain rate is proportional to the 3.67th moment [3]. Because the measurement of K_{DP} involves averaging over range, $R(K_{DP})$ may overestimate or underestimate rain rate due to the range averaging of differential phase (ϕ_{DP}) [3]. $R(Z_{HH}, Z_{DR})$ may give acceptable rain estimation for some cases, but it does not provide rain drop size distribution (DSD).

Accurate rain rate estimation requires detailed knowledge of rain DSD [3], [16]. In the past, rain DSD was commonly assumed to be an exponential distribution [17], [18]

$$n(D) = N_0 \exp(-\Lambda D) \qquad (0 < D < D_{\max}). \tag{1}$$

Exponential distribution has only two parameters (N_0, Λ), which may be inferred from Z_{HH} and Z_{DR}. Some observations, however, indicate that natural rain DSD contains fewer of both very large and very small drops than exponential distribution [19]–[21]. Ulbrich [19] suggested the use of the Gamma distribution for representing rain drop spectra as

$$n(D) = N_0 D^{\mu} \exp(-\Lambda D) \qquad (0 < D < D_{\max}). \tag{2}$$

The Gamma DSD with three parameters (N_0, μ, and Λ) is capable of describing a broader variation in rain drop size distribution than an exponential distribution, which is a special case of Gamma distribution with $\mu = 0$. It has been found that the three parameters are not mutually independent [19], [23]. Haddad *et al.* [23] parameterized rain DSD with transformed parameters that are uniformly random [24]. A normalized Gamma distribution was first proposed by Willis and recently adopted by Illingworth and Blackman to eliminate the dependence between N_0 and μ [25], [26]. The effort has concentrated on generating Gamma DSD from independent random variables.

For rain DSD retrieval however, the problem is how to retrieve the three parameters from limited radar measurements. Reflectivity and Z_{DR} are directly measured at every gate, whereas K_{DP} is the range derivative of ϕ_{DP}, the differential phase, over a number of gates. Thus gate-by-gate measurements of Z_{HH} and Z_{DR} cannot be combined with the range-smoothed K_{DP} for DSD retrieval. Therefore, only Z_{HH} and Z_{DR} are used for DSD parameter retrievals. An additional relation is needed for retrieving the three parameters of the Gamma distribution. An N_0–μ relation was used in Ulbrich's work on retrieving rain DSD from radar reflectivity and attenuation [19], but that relation is quite noisy in this study (see Section III-B).

In this paper, we propose a method for retrieving DSD parameters and use them to calculate rain rate and the characteristic size. The parameters are retrieved from radar measure-

Manuscript received December 30, 1999; revised June 8, 2000. The study was supported in part by the National Science Foundation, with funds designated for the U.S. Weather Research Program, National Center for Atmospheric Research (NCAR), Boulder, CO.

The authors are with the National Center for Atmospheric Research, Boulder, CO 80307-3000 USA (e-mail: vivek@ucar.edu).

Publisher Item Identifier S 0196-2892(01)02146-5.

ments Z_{HH} and Z_{DR}, and a constrained relation between μ and Λ derived from disdrometer observations. The paper is organized as follows. In Section II, simple closed-form expressions for polarimetric signatures of rain based on numerical calculation and curve-fitting of scattering amplitudes of raindrops are described. In Section III, we show results from video disdrometer measurements. The three parameters of Gamma DSD are obtained from three moments and then the μ–Λ relation is derived from the scatter plot. In Section IV, we present the method of retrieving the parameters from radar measurements. The results are compared with those based on the earlier published techniques. The proposed method shows improvement over the existing models. A summary of the proposed technique and discussion of results are given in Section V.

II. Theoretical Formulation

A complete theory of radar polarimetric signatures of hydrometeors (rain, hail, snow) can be found in previous studies [11], [3], [4]. In this section, we review the formulation and present closed-form expressions for polarimetric variables such as Z_{HH}, Z_{DR} and K_{DP} for a specified DSD and canting angle distribution.

The principle of polarimetric measurement is based on drops not being spherical but oblate in shape. The bigger the rain drop, the more oblate the shape. The relation between the shape parameter, the axis ratio between minor to major axis r, and the equivolume diameter D was given by Green [22]. By solving Green's equation and polynomial fitting, the following equation is obtained:

$$r = 1.0148 - 2.0465\times 10^{-2}D - 2.0048\times 10^{-2}D^2 + 3.095 \times 10^{-3}D^3 - 1.453\times 10^{-4}D^4 \quad (3)$$

where D is in mm.

When there is an electromagnetic wave incident on the spheroidal rain drop, wave scattering and propagation are different for horizontal and vertical polarizations. We first calculate the scattering amplitude of spheroidal rain drop at S-band of wavelength 10.7 cm based on the T-matrix method and Rayleigh scattering approximation. The dielectric constant of water is evaluated at a temperature of 10° C [27]. The scattering amplitudes are plotted as a function of the equivolume diameter D and shown in Fig. 1. Fig. 1(a) and (b) are backscattering amplitudes for polarization along major ($f_a(\pi)$) and minor ($f_b(\pi)$) axes, respectively. Fig. 1(c) and (d) show the corresponding forward-scattering amplitudes as a function of the equivolume diameter. The solid lines represent results using the T-matrix method, and dashed lines represent results calculated from Rayleigh scattering. We see good agreement between the two approaches except for very large drops ($D > 4$ mm). For the convenience of using these results for DSD retrieval, we fit the T-matrix results with the power-law function. The resultant magnitudes of the backscattering amplitudes ($f_{a,b}(\pi)$) and the real part of forward scattering amplitudes ($f_{a,b}(0)$) are as follows:

$$|f_a(\pi)| = \alpha_a D^{\beta_a} = 4.26\times 10^{-4}D^{3.02}\ \text{mm} \quad (4)$$

$$|f_b(\pi)| = \alpha_b D^{\beta_b} = 4.76\times 10^{-4}D^{2.69}\ \text{mm} \quad (5)$$

$$\text{Re}(f_a(0)) = \alpha'_a D^{\beta'_a} = 3.62\times 10^{-4}D^{3.27}\ \text{mm} \quad (6)$$

and

$$\text{Re}(f_b(0)) = \alpha'_b D^{\beta'_b} = 4.16\times 10^{-4}D^{2.91}\ \text{mm}. \quad (7)$$

The backscattering amplitudes are used for computing Z_{HH}, Z_{DR}, and Z_{DP}, whereas the difference between the real part of the forward-scattering amplitudes is used for computing K_{DP}. The difference between squares of the backscattering amplitudes can be written as

$$|f_a(\pi)|^2 - |f_b(\pi)|^2 = \alpha_d D^{\beta_d} = 1.44\times 10^{-8}D^{7.195}\ \text{mm}^2 \quad (8)$$

and the difference between the forward-scattering amplitudes is written as

$$\text{Re}(f_a(0) - f_b(0)) = \alpha_k D^{\beta_k} = 1.33\times 10^{-5}D^{4.61}\ \text{mm}. \quad (9)$$

Since rain media contains many randomly distributed particles, the total scattering amplitude is the sum of the individual scattering amplitude with relative phase taken into account. The wave statistics of the polarimetric measurements can be calculated based on ensemble averaging. The particle position, size, and orientation are randomly distributed. For simplification of derivation, we assume that the particle size and the orientation are statistically independent.

The second moment of scattering amplitude in horizontal polarization (HH) and vertical polarization (VV) can be obtained (see Appendix) as

$$\begin{aligned}\langle|F_{hh}|^2\rangle &= (1-2\sigma_\phi^2)\langle|f_a(\pi)|^2\rangle + 2\sigma_\phi^2\langle f_a(\pi)f_b(\pi)^*\rangle \\ &= N_0[(1-2\sigma_\phi^2)\alpha_a^2\Lambda^{-(2\beta_a+\mu+1)}\Gamma(2\beta_a+\mu+1) \\ &\quad + 2\sigma_\phi^2\alpha_a\alpha_b\Lambda^{-(\beta_a+\beta_b+\mu+1)}\Gamma(\beta_a+\beta_b+\mu+1)] \\ &\quad \text{mm}^2\text{m}^{-3}\end{aligned} \quad (10)$$

$$\begin{aligned}\langle|F_{vv}|^2\rangle &= (1-2\sigma_\phi^2)\langle|f_b(\pi)|^2\rangle + 2\sigma_\phi^2\langle f_a(\pi)f_b(\pi)^*\rangle \\ &= N_0[(1-2\sigma_\phi^2)\alpha_b^2\Lambda^{-(2\beta_b+\mu+1)}\Gamma(2\beta_b+\mu+1) \\ &\quad + 2\sigma_\phi^2\alpha_a\alpha_b\Lambda^{-(\beta_a+\beta_b+\mu+1)}\Gamma(\beta_a+\beta_b+\mu+1)] \\ &\quad \text{mm}^2\text{m}^{-3}\end{aligned} \quad (11)$$

where the $\langle\cdots\rangle$ represents an ensemble average. In above equations, σ_ϕ is the standard deviation of the canting angle.

For dual-polarization radar measurements, the reflectivity at horizontal (Z_{HH}) and vertical polarization (Z_{VV}) can be expressed as

$$\begin{aligned}Z_{HH} &= \frac{4\lambda^4}{\pi^4|K_w|^2}\langle|F_{hh}|^2\rangle \\ &= \frac{4\lambda^4}{\pi^4|K_w|^2}N_0\Lambda^{-(\mu+1)} \\ &\quad [(1-2\sigma_\phi^2)\alpha_a^2\Lambda^{-2\beta_a} \\ &\quad \cdot\Gamma(2\beta_a+\mu+1) \\ &\quad + 2\sigma_\phi^2\alpha_a\alpha_b\Lambda^{-\beta_a-\beta_b} \\ &\quad \cdot\Gamma(\beta_a+\beta_b+\mu+1)]\,\text{mm}^6\text{m}^{-3}\end{aligned} \quad (12)$$

and

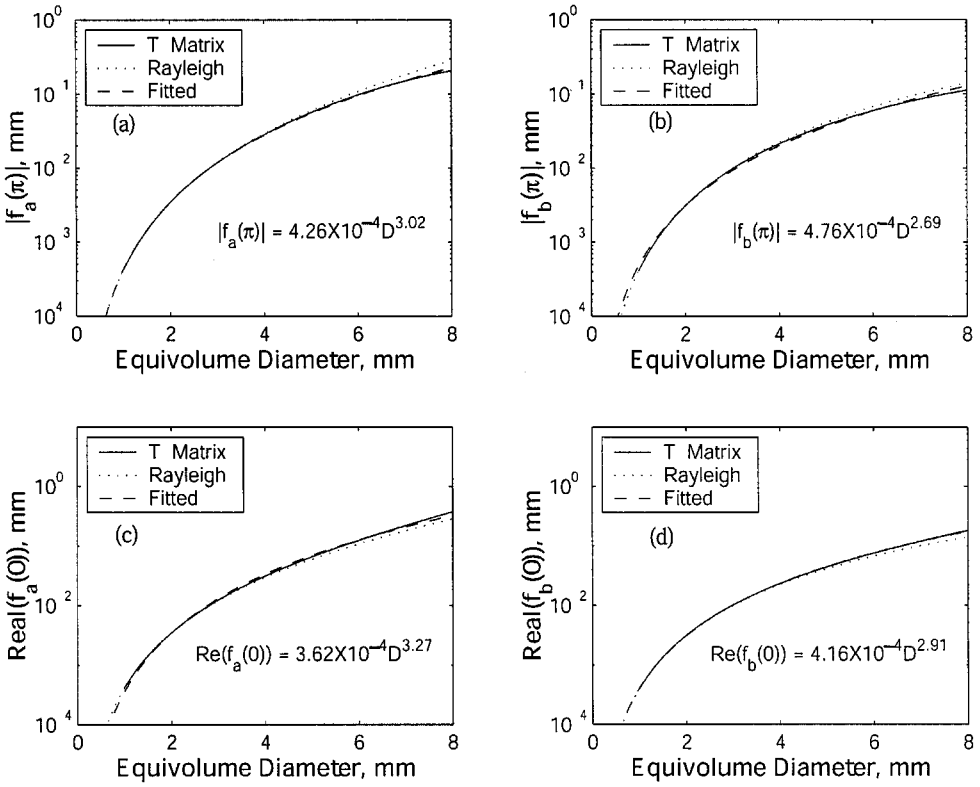

Fig. 1. Polarimetric scattering amplitudes as a function of particle size [effective diameter (D_0)]. (a) Backscattering amplitude for major axis, (b) backscattering amplitude for minor axis, (c) forward-scattering amplitude for major axis, and (d) forward-scattering amplitude for minor axis.

$$\begin{aligned} Z_{VV} &= \frac{4\lambda^4}{\pi^4|K_w|^2}\langle|F_{vv}|^2\rangle \\ &= \frac{4\lambda^4}{\pi^4|K_w|^2} N_0\Lambda^{-(\mu+1)} \\ &\quad [(1-2\sigma_\phi^2)\alpha_b^2\Lambda^{-2\beta_b} \\ &\quad \cdot\Gamma(2\beta_b+\mu+1) \\ &\quad + 2\sigma_\phi^2\alpha_a\alpha_b\Lambda^{-\beta_a-\beta_b} \\ &\quad \cdot\Gamma(\beta_a+\beta_b+\mu+1)]\ \text{mm}^6\text{m}^{-3}. \end{aligned} \tag{13}$$

The dielectric factor $K_w = (\epsilon_r - 1)/(\epsilon_r + 2)$, ϵ_r is the complex dielectric constant, and λ is the wavelength in meters. The reflectivity difference is

$$Z_{DP} = Z_{HH} - Z_{VV} \tag{14}$$

and the reflectivity ratio is

$$Z_{DR} = Z_{HH}/Z_{VV}. \tag{15}$$

The specific differential phase [14] is

$$\begin{aligned} K_{DP} &= \frac{180\lambda}{\pi}(1-2\sigma_\phi^2)\langle\text{Re}[f_a(0)-f_b(0)]\rangle \\ &= \frac{180\lambda}{\pi}(1-2\sigma_\phi^2)N_0\alpha_k\Lambda^{-(\beta_k+\mu+1)}\Gamma(\beta_k+\mu+1) \\ &\quad \text{degree km}^{-1}. \end{aligned} \tag{16}$$

III. Disdrometer Observations

Application of the polarimetric radar technique for estimating precipitation has been evaluated in various field experiments. Data used in this study were collected in east-central Florida during the summer of 1998 when NCAR's S-Pol radar was deployed in a special experiment (PRECIP98) to evaluate the potential of polarimetric radar for estimating rain in a tropical environment. The experiment was conducted in conjunction with the National Aeronautics and Space Administration (NASA) Tropical Rain Measuring Mission (TRMM).

Here we compare S-Pol radar measurements and raindrop observations from a video disdrometer [34]. The 3 dB beamwidth of S-Pol is 0.92° and the radar data were collected at 1° elevation angle. The disdrometer was located at an azimuth of 315° and a range of 38 km from the radar. Drops were quantized into size categories of 0.05 or 0.2 mm at 1 min intervals. The observations include drop concentrations, the number of drops within each size category, and their mean terminal velocity.

A. Fitting the DSD with a Gamma Distribution

The measured DSD can be fitted with a Gamma distribution by curve-fitting or matching moments. The moment method has been widely accepted in the meteorology community [20], [21]. For a Gamma distribution, the nth moment is

$$\langle D^n\rangle = \int D^n n(D)dD = N_0\Lambda^{-(\mu+n+1)}\Gamma(\mu+n+1). \tag{17}$$

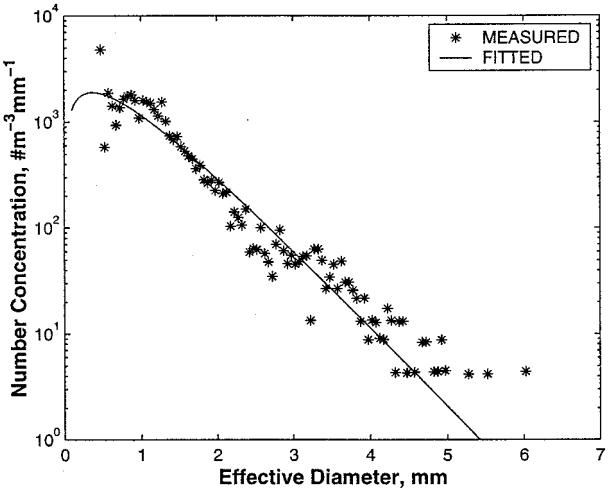

Fig. 2. Example of rain DSD and its fitted Gamma distributions. Asterisks: Disdrometer measurements. Solid line: fitted Gamma distribution using second, fourth, and sixth moments.

In general, the three parameters (N_0, μ, and Λ) can be solved from any three moments. Tokay and Short [21] used the third, fourth, and sixth moments. The results are shown in Fig. 2. The solid line is from the method of using the second, fourth, and sixth moments. It fits the measurement well and gives a consistent rain rate estimation. The rain rate from the measured DSD is 74.9 mm hr^{-1}, and the calculated rain rate from the fitted DSD is 71.9 mm hr^{-1}. We use the moment method to fit the measured DSD with Gamma distribution since the three moments directly correspond to radar measurements Z_{HH}–$\langle D^6\rangle$, K_{DP}–$\langle D^{4.61}\rangle$, which is close to $\langle D^4\rangle$, and the scattering cross section at the geometrical optics region $\langle D^2\rangle$.

B. Relations Among DSD Parameters

To find relations among the three parameters of Gamma DSD, we plot N_0 versus μ, N_0 versus Λ, and μ versus Λ, and show the result in Fig. 3(a)–(c), respectively. Both N_0–μ and N_0–Λ plots are highly scattered, while high correlation exists in the μ–Λ plot. Dependencies of μ and Λ on rain rate (R), and the relation between rain rate and median volume diameter (MVD), are shown in Fig. 4. Again, there is little correlation between R and μ, and R and Λ. We notice that the large values of μ and Λ (> 15) correspond to low rain rate ($R < 5$ mm hr^{-1}). Polarimetric measurements are more sensitive to heavy rain than to light rain. Thus, in Fig. 5, we plot N_0–μ and μ–Λ for the cases ($R > 5$ mm hr^{-1}). N_0 has better correlation with μ than that shown in Fig. 3(a), but the scatter between them is large with a correlation coefficient of 0.85 compared to the scatter between μ versus Λ. For a given $\mu = 2$, N_0 ranges from 10^3 to 10^5, which is more than ten times different from the fitted value. The relation for μ versus Λ is found by using polynomial curve-fitting, which has a correlation of 0.97, as given by

$$\mu = -0.016\Lambda^2 + 1.213\Lambda - 1.957. \tag{18}$$

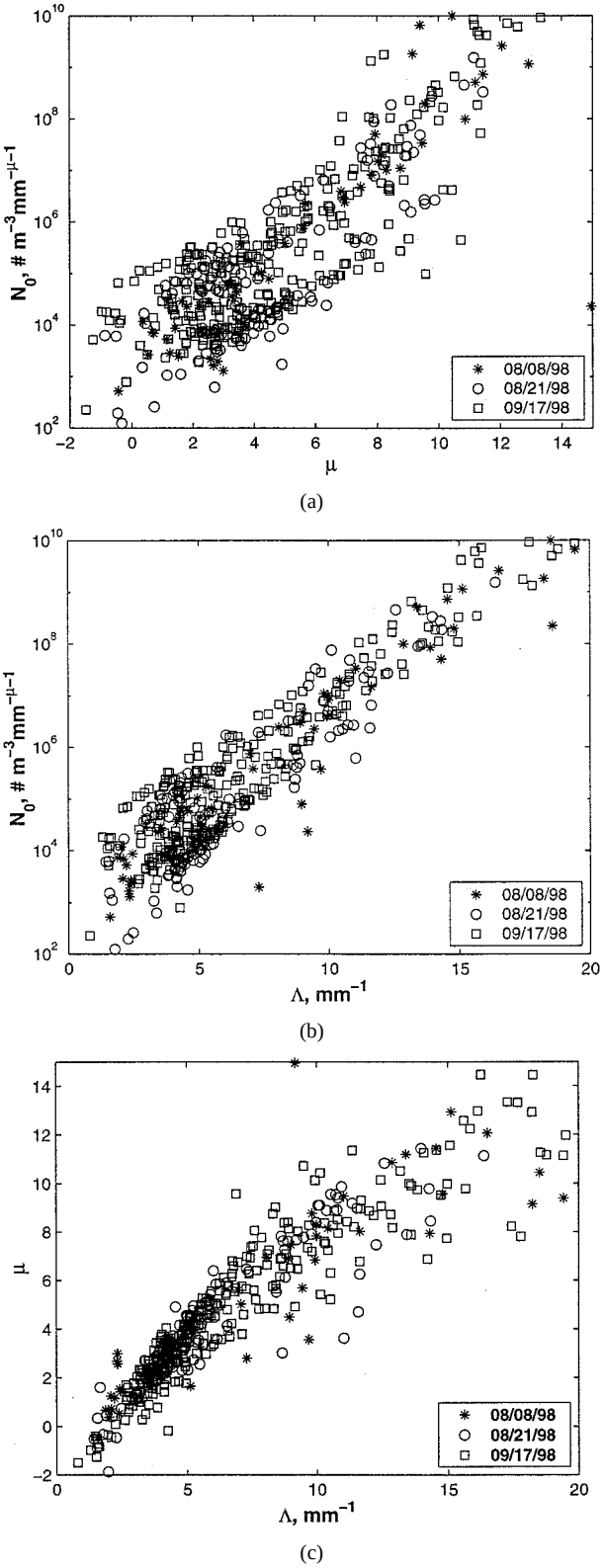

Fig. 3. Scatter plots of the Gamma DSD parameters. (a) N_0 versus μ, (b) N_0 versus Λ, and (c) μ versus Λ.

The video disdrometer measurements included convective and stratiform precipitation. Equation (18) is very similar to that derived from DSD measurements in Darwin, Australia, [28], and in good agreement with the DSD observations μ–Λ in other studies [21], [29]–[31]. DSD parameters measured

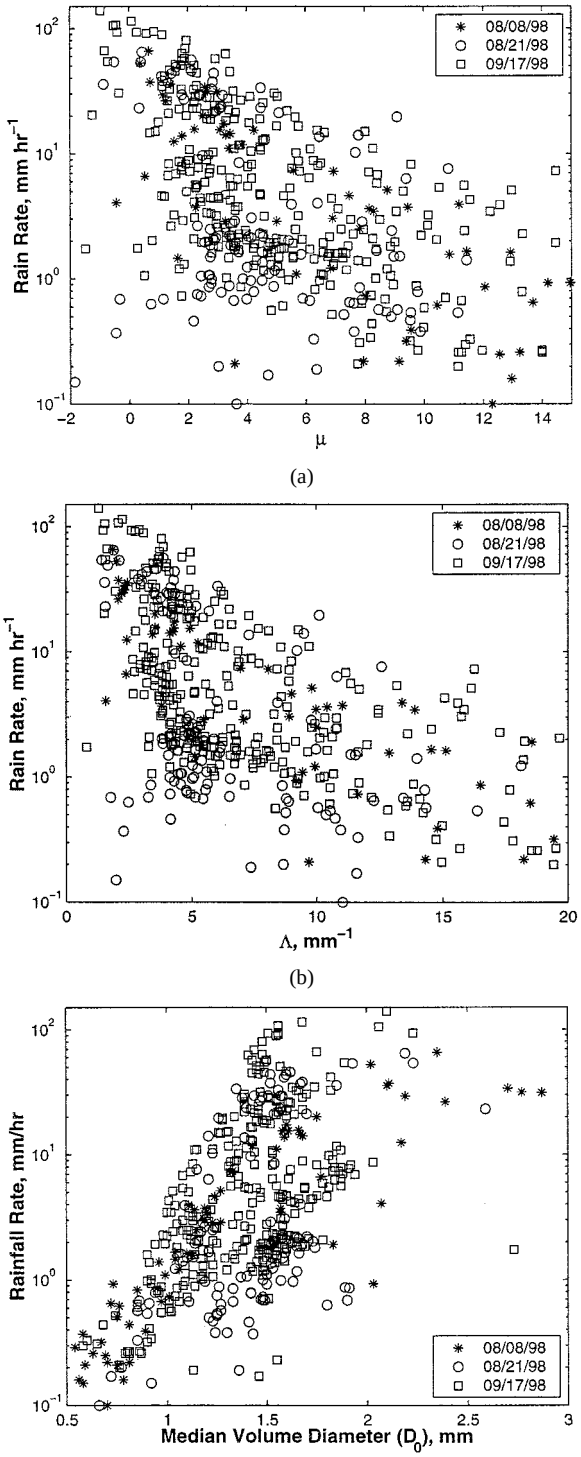

Fig. 4. Scatter plots of rain rate versus DSD parameters. (a) R versus μ, (b) R versus Λ, and (c) R versus D_0.

in various geographical locations show reasonable agreement with the μ–Λ relation obtained in Florida rain events as shown in Fig. 5(c). Equation (18) suggests that irrespective of rain intensity or rain type (convective or stratiform), DSD parameters exhibit the following characteristics: 1) large (small) μ corresponds to narrow (broad) distribution, and 2) large (small) Λ corresponds to small (large) MVD and narrow (broad) distribution.

IV. DSD Parameter Retrievals and Rain Rate Estimation

The μ–Λ relation (18) combined with the Z_{HH} and Z_{DR} constitute the three equations for retrieving the three Gamma DSD parameters. Datasets selected for analysis were obtained on August 8 and 21 and September 17 during PRECIP98. Radar samples were made at intervals of 20 s to 2 min and had a spatial resolution of 0.15 km. The azimuthal dimension of the radar beam at the video disdrometer location is 0.61 km. Precipitation echo might advance 0.5 to 1 km in a minute. To reduce the uncertainty in the radar measurements the data were averaged over five range gates. And when more than one radar observation was taken during the 1 min sampling period of the disdrometer, the radar data were also averaged in time. Comparisons between the radar and the disdrometer are for the range bin that includes the disdrometer. In the next section, we illustrate the retrieving procedure and compare the results with those obtained using different techniques.

A. Parameter Retrievals

In the case of a two parameter (exponential) DSD, reflectivity and differential reflectivity observations can be used for estimating N_0 and Λ [1], [2]. As shown in the previous section, the dependency between μ and Λ reduces the three parameter Gamma DSD to a two parameter function, which we refer to as a constrained Gamma DSD. Thus, Z_{HH} and Z_{DR} can be used to infer the two parameters. Fig. 6 shows the relations of Z_{DR} versus Λ and Z_{HH}/N_0 versus Λ for the constrained Gamma DSD. For a specified Z_{DR}, Λ can be inferred and then using the inferred Λ and Z_{HH}, the parameter N_0 can be obtained. This procedure is implemented as follows.

Step 1) Use an iteration method for retrieving Λ and μ from the coupled equations of (15) and (18).

Step 2) Find N_0 from (12) with a specific Λ, μ, and Z_{HH}.

B. Rain Rate Estimation and Comparison

Once the rain DSD is known, the rain rate can be calculated as

$$R = \frac{\pi}{6}\int_0^{D_{\max}} D^3 N(D) v(D)\, dD. \tag{19}$$

For the video disdrometer measurement, the drop spectrum $n(D)$ and the terminal velocity $v(D)$ are directly measured, and the rain rate is calculated using (19). Rain rate is computed for every 1 min sample of disdrometer observation.

For radar measurements, the rain rate can be obtained either by retrieving the DSD (as discussed above) or using empirical relations. The terminal velocity is assumed [3] as

$$v(D) = 3.778 D^{0.67} \qquad (\text{in ms}^{-1} \text{ for } D \text{ in mm}) \tag{20}$$

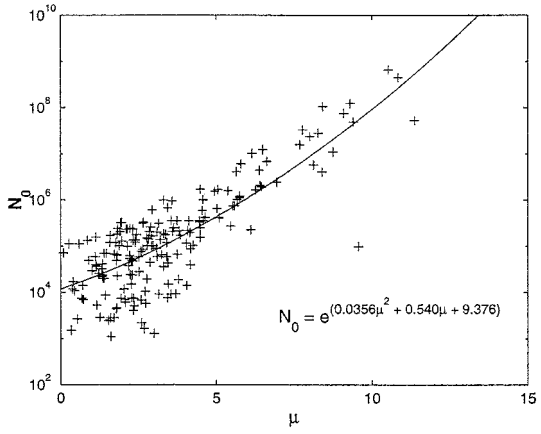

(a)

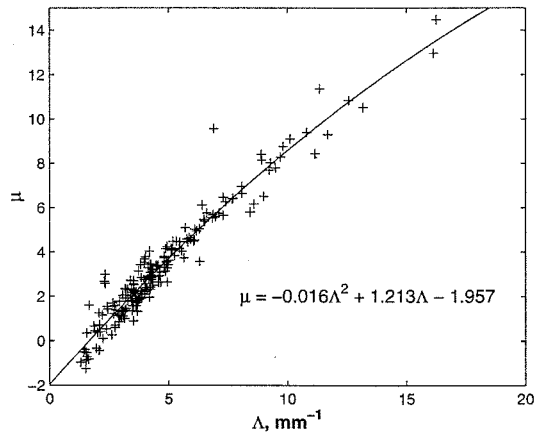

(b)

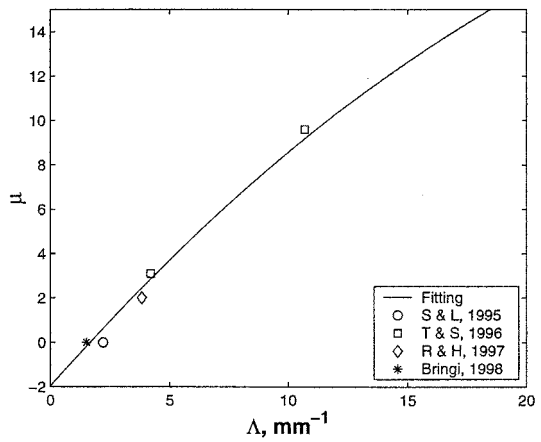

(c)

Fig. 5. Relations among Gamma DSD Parameters for high rain rate cases ($R > 5$ mm/hr). (a) N_0 versus μ, (b) μ versus Λ, and (c) μ versus Λ from previous observations.

and the rain rate can be calculated by substituting (2) and (20) into (19) and performing the integration

$$R = 7.125 \times 10^{-3} N_0 \Lambda^{-(3.67+\mu+1)} \Gamma(3.67+\mu+1) \text{ mm hr}^{-1}. \tag{21}$$

Traditionally, the rain rate is estimated by using empirical relations. The NEXRAD $R(Z)$ is

$$R(Z) = (Z_{HH}/300)^{1/1.4} \text{ mm hr}^{-1}. \tag{22}$$

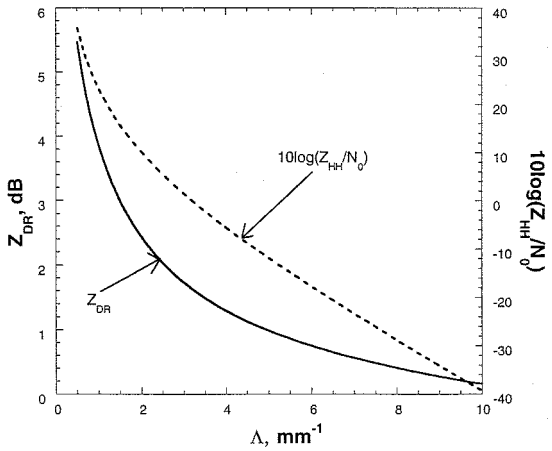

Fig. 6. Dependencies of Z_{DR} and $10\log(Z_{HH}/N_0)$ on Λ.

TABLE I
MEAN RAIN RATE COMPARISON

Event	Video	Gamma	$R(Z_{HH}, Z_{DR})$	$R(Z_{HH})$	$R(K_{DP})$
8/8/98	10.2	8.0	10.1	6.5	10.1
8/21/98	21.6	26.6	33.5	17.5	12.3
9/17/98	28.7	25.7	37.8	15.1	22.2

Rain rate estimation based on Z and Z_{DR} is [15]

$$R(Z, Z_{DR}) = 6.86 \times 10^{-3} Z_{HH} Z_{DR}^{-4.86} \text{ mm hr}^{-1}. \tag{23}$$

Rain rate estimation based on K_{DP} is [15]

$$R(Z) = 40.56 K_{DP}^{0.866} \text{ mm hr}^{-1}. \tag{24}$$

S-Pol is a well calibrated radar system. Bias error in dBZ measurement is known within 1 dB. Standard errors in Z, Z_{DR} and ϕ_{DP} are ± 1 dB, ± 0.2 dB, and $\pm 0.3°$, respectively, for a typical spectral width of 2 ms^{-1} [3]. The results for the rain rate estimation during the PRECIP98 experiment are shown in Fig. 7. Fig. 7(a) and (b) are taken from 19:06:00 to 19:41:00 on August 8, 1998, in which we see a mismatch between video disdrometer and radar-based peak rain rate. The mismatch might be due to the sampling and the radar beam offset. Fig. 7(c) and (d) shows the results for a period (14:20:00 to 15:00:00) on August 21, 1998. Good agreement can be seen between video disdrometer measurement and the constrained Gamma retrievals from radar measurement. Fig. 7(e) and (f) show the results for the period 21:21:00 to 21:41:00 on September 17, 1998. The constrained Gamma retrievals give a reasonable rain estimation compared with other methods. Since rain rates fluctuate during this period and the sampling problem (mismatch between disdrometer location and radar sensing volume) introduces uncertainty, the mean rain rates are computed for the entire period. Table I shows the comparisons of the mean rain rates obtained with the five different methods.

The estimators $R(Z, Z_{DR})$, $R(Z)$, and $R(K_{DP})$ were derived from simulation results with MVD varying between 0.5 and 2.5 mm [15]. The video disdrometer observations indicate MVD is 1.5 mm. The results shown in Table I indicate that $R(Z)$

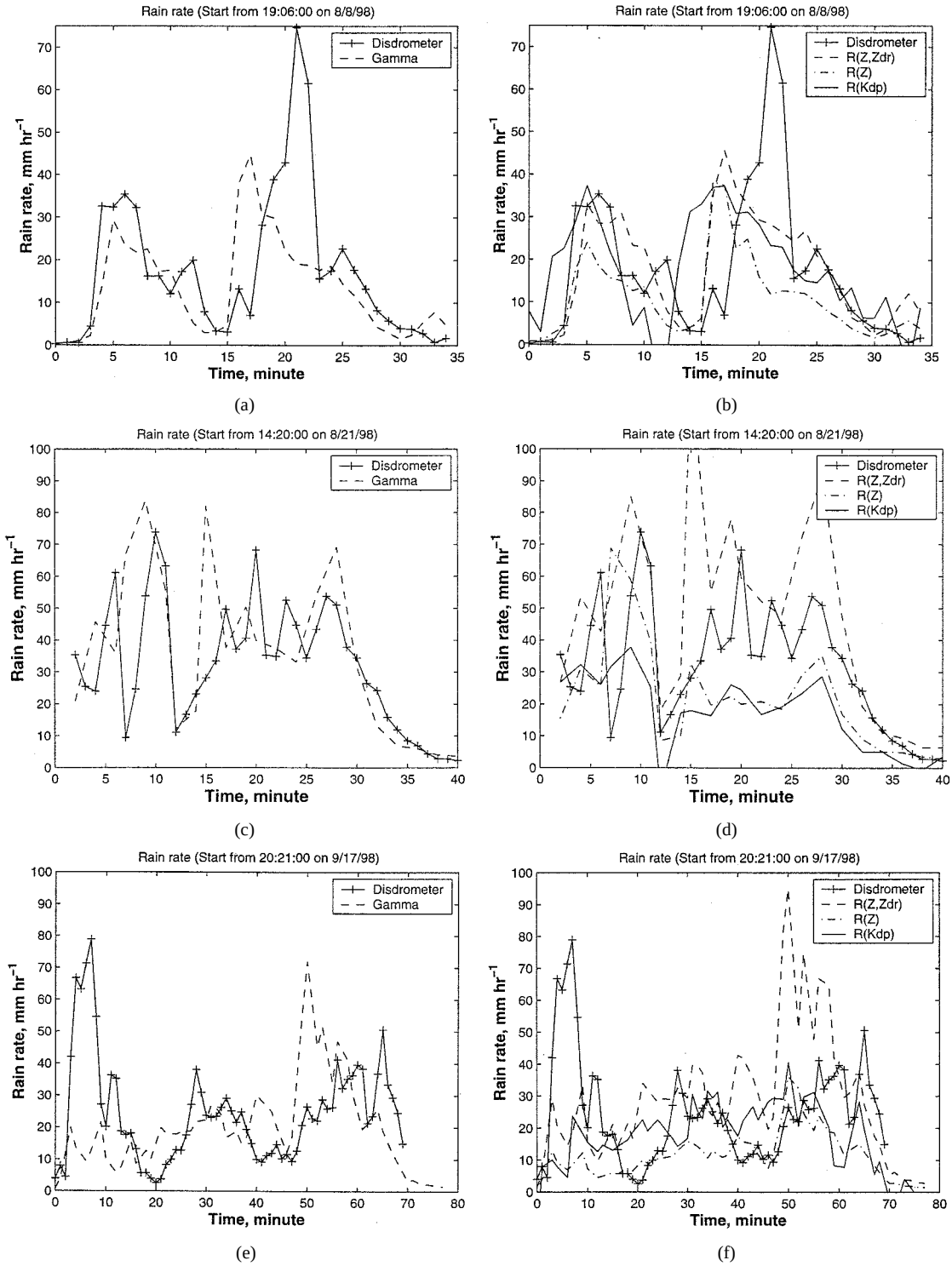

Fig. 7. Comparison of rain rates obtained using different methods for three time periods. (a) Gamma DSD retrieval for 19:06:00–19:41:00 on 8/8/98, (b) empirical relations for 19:06:00–19:41:00 on 8/8/98, (c) gamma DSD retrieval for 14:20:00–15:00:00 on 8/21/98, (d) empirical relations for 14:20:00–15:00:00 on 8/21/98, (e) gamma DSD retrieval for 20:21:00–21:40:00 on 9/17/98, and (f) empirical relations for 20:21:00–21:40:00 on 9/17/98.

and $R(K_{DP})$ generally underestimate and $R(Z, Z_{DR})$ overestimate rain rate for the rain events in PRECIP98 with smaller medium volume diameters (MVDs). It is interesting to note that good agreement among $R(K_{DP})$, $R(Z, Z_{DR})$, and video observation on 8 August 1998 is due to the presence of MVDs > 2 mm [see Fig. 4(c)]. In general, the constrained Gamma retrievals are in better agreement with the disdrometer measurements.

C. Characteristic Size Retrieval and Comparison

In addition to rain rate, MVD of rain is another important parameter to characterize rain. To our knowledge, only limited results of MVD retrieval using polarization measurement have been published except for the exponential DSD. With the method of

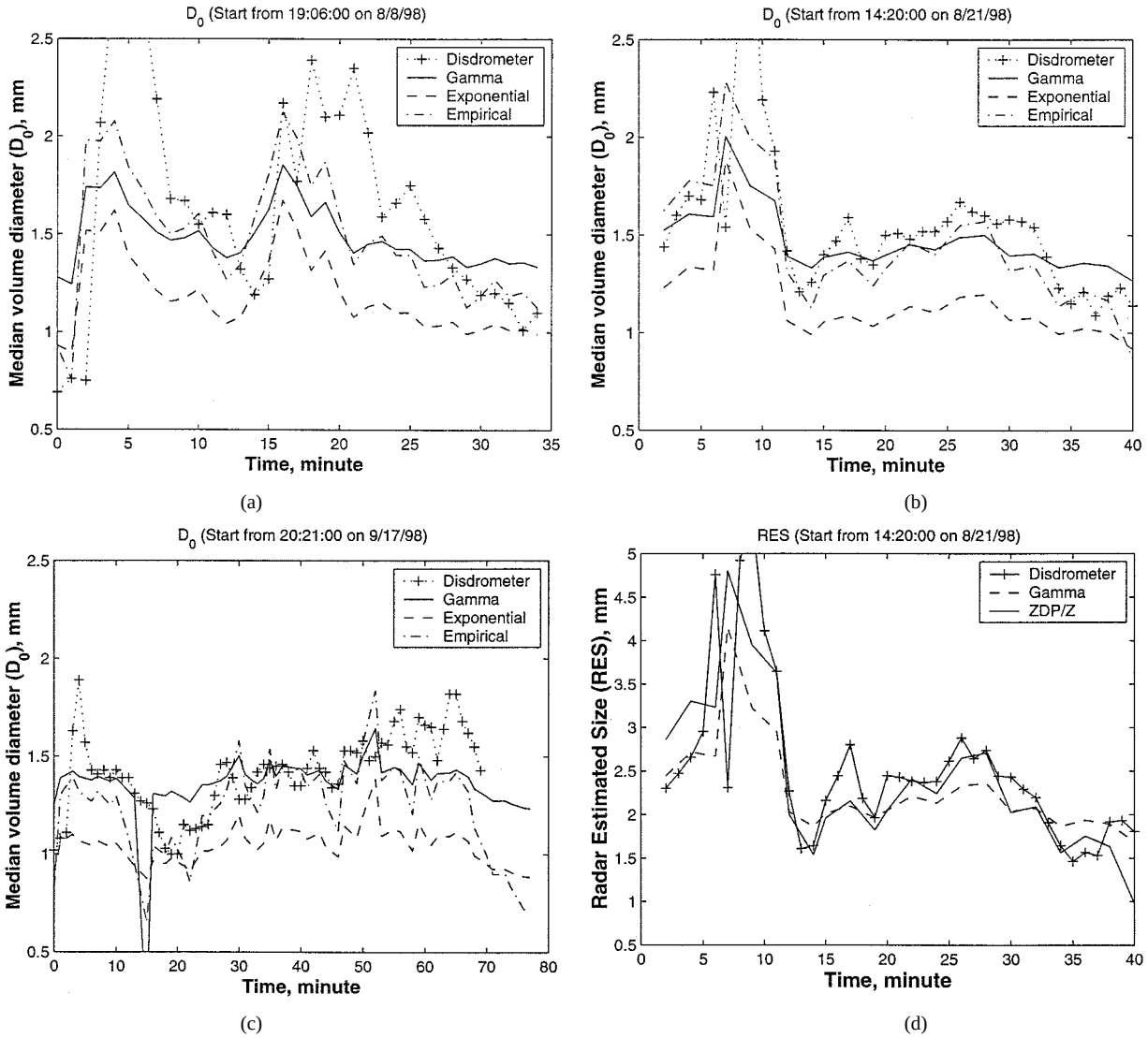

Fig. 8. Comparison of characteristic size obtained using different methods for three time periods. (a) MVD for 19:06:00–19:41:00 on 8/8/98, (b) MVD for 14:20:00–15:00:00 on 8/21/98, (c) MVD for 20:21:00–21:40:00 on 9/17/98, and (d) RES for 14:20:00–15:00:00 on 8/21/98.

constrained Gamma DSD retrieval, we are able to calculate the MVD using the retrieved μ and Λ from Z_{DR} as

$$D_0 = (\mu + 3.67)/\Lambda. \tag{25}$$

Empirically, MVD is directly estimated from Z_{DR} (in dB units) [32] as

$$D_0 = 1.529 Z_{DR}^{0.467} \text{ mm}. \tag{26}$$

The disdrometer-measured and retrieved MVDs are shown in Fig. 8(a)–(c). The dot-plus line is from the disdrometer measurement. The solid line shows the radar retrieved value using the constrained Gamma DSD retrieval. The dashed line is that retrieved based on exponential DSD. The dot-dash line is obtained from the empirical relation (26). Fig. 8(a) again shows the mismatch between video and radar measurement. Fig. 8(b) and (c) shows that the constrained Gamma retrievals agree with disdrometer measurements, that the retrievals are much better than exponential DSD retrievals and that they are a little better than the empirical result. The mean differences of the Gamma DSD retrievals from the disdrometer measurement are 0.164, 0.104, and 0.153 mm, while the exponential DSD retrievals are 0.464, 0.408, and 0.360 mm, respectively. The mean error is reduced to 1/3 by using constrained Gamma DSD. The mean differences for the empirical relation are 0.162, 0.122, and 0.221 mm, which are larger (on average) than those from constrained Gamma DSD.

We notice that the MVD cannot be obtained unless rain DSD has been retrieved or an empirical relation is used. As shown in Section II, the reflectivity difference is proportional to the 7.195th moment of DSD based on the power-law fitted relations (8). It is well known that S-band reflectivity of rain is close to the sixth moment. The ratio of Z_{DP} and Z_{HH} can be used to define a characteristic size of raindrops. Thus, a new parameter, namely, radar estimated size (RES) for rain DSD can be defined as

$$\text{RES} = \left[\frac{\langle D^{\beta_d}\rangle}{\langle D^{2\beta_a}\rangle}\right]^{1/(\beta_d - 2\beta_a)} = C_1 \left(\frac{Z_{DP}}{Z_{HH}}\right)^{C_2}. \tag{27}$$

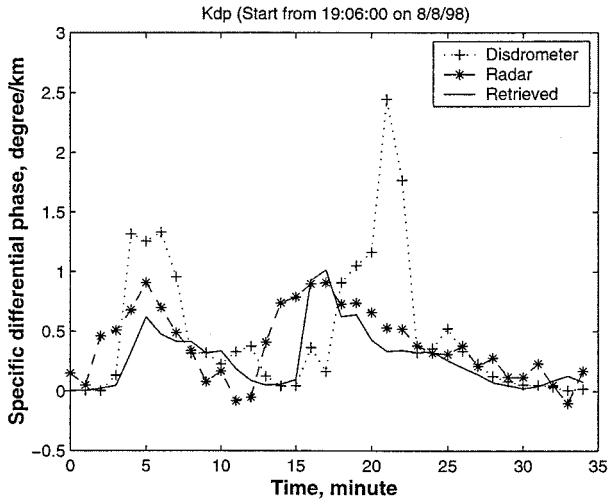

(a)

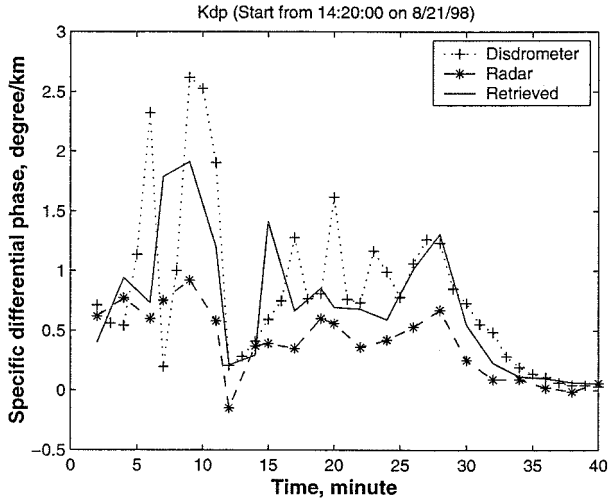

(b)

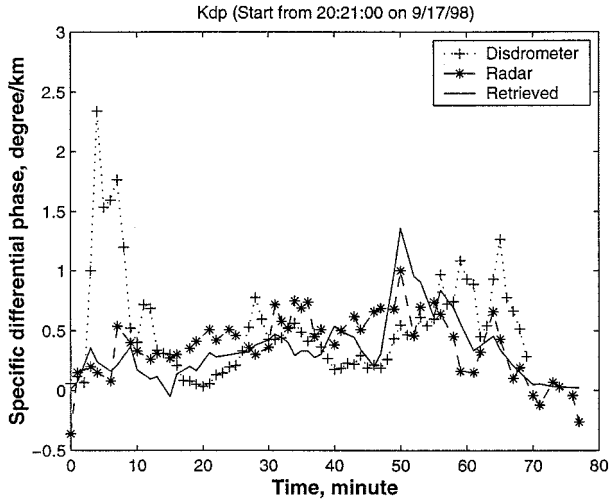

(c)

Fig. 9. Comparison of specific phase differences obtained using different methods for three time periods. (a) 19:06:00–19:41:00 on 8/8/98, (b) 14:20:00–15:00:00 on 8/21/98, and (c) 20:21:00–21:40:00 on 9/17/98.

The constants C_1 and C_2 can be estimated from the power-law fitted relations (4) and (8) and have values of (8.97, 0.866) for $\sigma_\phi = 5^\circ$ and (10.19, 0.866) for $\sigma_\phi = 15^\circ$, respectively. For a narrow DSD, the MVD and RES can be the same. In the case of a broad distribution, the RES can be a lot larger than MVD. An RES retrieval is shown in Fig. 8(d). The solid-plus line represents disdrometer measurements. The solid line is the radar retrieved value based on the Z_{DP}–Z_{HH} ratio (27), and the dashed line is the result calculated from the retrieved Gamma DSD. We see good agreement among all three approaches. The advantage of using RES instead of MVD is that the particle size can be obtained without knowing the DSD.

D. Comparison Between Measured and Retrieved K_{DP}

In the constrained Gamma DSD retrieval, K_{DP} is not used because of the smearing effect from gate to gate that results from filtering. K_{DP}, however, can be measured using a polarimetric radar, and it is widely used for rain rate estimation. In this subsection, we calculate K_{DP} using disdrometer measured DSD and the retrieved DSD inferred from Z_{HH} and Z_{DR} and compare them with radar measurements.

The K_{DP} results are shown in Fig. 9. The dotted line with plus signs represents the calculated results from the disdrometer measured DSD. The dashed line with asterisks represents the radar K_{DP}. The solid line represents the calculated K_{DP} from the retrieved Gamma DSD based on radar measured Z_{HH} and Z_{DR}. The K_{DP} from the retrieved Gamma DSD captures the measured results well and has higher peaks than the measured value. The large K_{DP} values agree well with those calculated from video disdrometer measured DSD [Fig. 9(b)]. This is expected because the measured K_{DP} is derived from low-pass filtering of ϕ_{DP}, which smears the high K_{DP} values. The retrieved Gamma DSD, however, is obtained from Z_{HH} and Z_{DR} for a single range gate.

V. Summary and Discussions

In this paper, we propose a method of retrieving rain DSD from polarimetric radar measurements. A constrained (μ–Λ) relation derived from disdrometer observations is used in retrieving a Gamma distribution. DSD parameters exhibit the following characteristics: 1) large (small) μ corresponds to a narrow (broad) distribution, and 2) large (small) Λ corresponds to small (large) MVD and narrow (broad) DSD. The Gamma DSD parameters (N_0, μ, and Λ) are retrieved from radar measurements (Z_{HH} and Z_{DR}) and the constrained relation. Rain rate, particle size, and K_{DP} are calculated and compared with that obtained from disdrometer measured DSDs. The constrained Gamma DSD retrieval has the following advantages over existing methods: 1) it allows the three parameter Gamma DSD to be retrieved and the shape of DSD to be obtained, 2) it gives a better estimation of MVD than the exponential DSD model; and 3) the DSD-based K_{DP} has sharper peaks than radar measured K_{DP} due to range averaging of ϕ_{DP} profile. The closed-form expressions for reflectivity, specific propagation phase, and differential reflectivity were obtained using rigorous scattering calculations. The expressions depend on both size and canting angle distribution parameters.

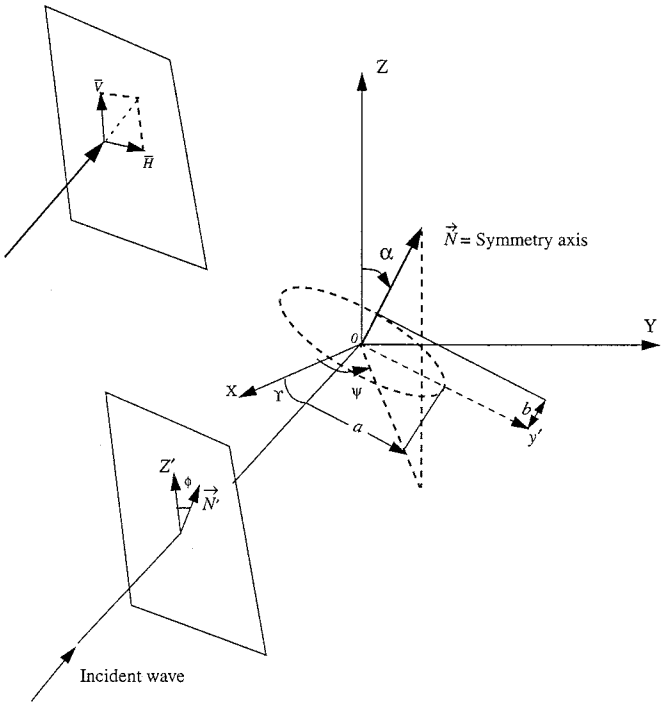

Fig. 10. Scattering geometry where $\overline{N}$ is the symmetry axis of the scatterer. $\overline{N'}$ and $\overline{Z'}$ are projections of the $\overline{N}$ and $\overline{Z}$ axes onto the polarization plane. Angles ϕ and γ are the components of the true canting angle α. $\overline{V}$ and $\overline{H}$ are the linear polarization base vectors.

The constrained relation used in this paper was derived from disdrometer observations taken from Florida rain events. This relation may change for different locations or seasons, in which case the coefficient might have to be adjusted. Errors from the curve fitting and integration depend on the rain DSD. The errors are larger for a broader DSD and smaller for a narrower DSD. For example, the error from fitting is within 2% and that from integration is within 3% for a DSD of $D_0 = 1.5$ mm and $\mu > 2$. The integration over particle size within a finite region can be performed by using incomplete Gamma function. The mismatches in the comparisons of rain rate and drop size might be due to huge difference in sampling volumes between radar and disdrometer. Nevertheless, ground-based gauge or disdrometer is used as a standard comparison. Variation in agreement between radar and disdrometer might also depend on advection of the precipitation and finite sampling interval of radar and video disdrometer (1 min). In this study, no correction is made for movement of the storm. In this paper, Green's equilibrium model has been used to calculate the axis ratio of raindrops. The effect of particle shape on rain estimation will be investigated in future work. However, the retrieval technique is a general method and combines both radar and ground-based observations for more accurate rain estimation.

Appendix
Derivation of the Second Moments of Scattering Amplitudes for Canting Raindrops

Consider an oblate spheroidal particle (as shown in Fig. 10) with a symmetric axis ON, major and minor semi-axes a and b. For the incident polarization of the wave aligned along the major and minor axis, the cross-polarization term is zero and the scattering matrix ($\overline{\overline{f}}$) is diagonal as

$$\overline{\overline{f}} = \begin{bmatrix} f_a & 0 \\ 0 & f_b \end{bmatrix} \tag{A.1}$$

where f_a and f_b are proportional to the horizontal and vertical scattering cross sections of the oblate spheroid, respectively.

For a wave incident at an elevation angle (γ) from the symmetric axis, Rayleigh scattering amplitude can be approximated [35] as

$$\begin{aligned} f'_h(\gamma) &= f_a \\ f'_v(\gamma) &= f_a \cos^2\gamma + f_b \sin^2\gamma. \end{aligned} \tag{A.2}$$

For a canting angle (ϕ) between $\hat{N}$ and $\hat{Z}'$ in the polarization plane, the laboratory and body coordinate referenced electric fields are related as

$$\begin{bmatrix} E_h \\ E_v \end{bmatrix} = \begin{bmatrix} \cos\phi & \sin\phi \\ -\sin\phi & \cos\phi \end{bmatrix} \begin{bmatrix} E'_h \\ E'_v \end{bmatrix}. \tag{A.3}$$

Thus, in the laboratory coordinates (x, h, v), the backscattering matrix for an arbitrarily canted raindrop can be expressed as a function of the principal scattering amplitude (f_a, f_b) as

$$\begin{aligned} \begin{bmatrix} f_{hh} & f_{hv} \\ f_{vh} & f_{vv} \end{bmatrix} &= \begin{bmatrix} \cos\phi & -\sin\phi \\ -\sin\phi & \cos\phi \end{bmatrix} \begin{bmatrix} f'_h & 0 \\ 0 & f'_v \end{bmatrix} \\ &\quad \cdot \begin{bmatrix} \cos\phi & \sin\phi \\ -\sin\phi & \cos\phi \end{bmatrix} \\ &= \begin{bmatrix} Af_a + Bf_b & (f_a - f_b)\sqrt{BC} \\ (f_a - f_b)\sqrt{BC} & Cf_b + Df_a \end{bmatrix} \end{aligned} \tag{A.4}$$

where

$$\begin{aligned} A &= \cos^2\phi + \sin^2\gamma \sin^2\phi \\ B &= \cos^2\gamma \sin^2\phi \\ C &= \cos^2\gamma \cos^2\phi \\ D &= \sin^2\phi + \sin^2\gamma \cos^2\phi \end{aligned}$$

and ϕ and γ are canting angle components in polarization and transverse planes, respectively.

Radar resolution volumes contain a collection of particles that are randomly distributed, and the corresponding total scattering amplitude is

$$F_{pq} = \sum_{l=1}^{N} f_{pq}^{(l)} e^{i\overline{k}_d \cdot \overline{r_l}} \tag{A.5}$$

where $p, q = v$, or h and $k_d = 2(2\pi/\lambda)$, $\overline{r_l}$ is the position of the lth scatterer. The above described scattering amplitude can be used to obtain various co- and cross covariances as shown in (A.7)

$$\begin{aligned} \langle |F_{hh}|^2 \rangle &= \langle (Af_a + Bf_b)(Af_a + Bf_b)^* \rangle \\ &= \overline{A^2}\langle |f_a|^2 \rangle + \overline{B^2}\langle |f_b|^2 \rangle + 2\overline{AB}\langle f_a f_b^* \rangle \end{aligned} \tag{A.6}$$

$$\begin{aligned} \langle |F_{vv}|^2 \rangle &= \langle (Cf_b + Df_a)(Cf_b + Df_a)^* \rangle \\ &= \overline{D^2}\langle |f_a|^2 \rangle + \overline{C^2}\langle |f_b|^2 \rangle + 2\overline{CD}\langle f_a f_b^* \rangle \end{aligned} \tag{A.7}$$

where the $\langle \cdots \rangle$ represents the integration over droplet size, and — is the average over orientation. It is assumed that orientation and particle distributions are statistically independent. For

small canting angle and elevation angle, we have approximated expressions for co-pol scattering as follows:

$$\langle|F_{hh}|^2\rangle \cong (1-2\sigma_\phi^2)\langle|f_a|^2\rangle + 2\sigma_\phi^2\langle f_a f_b^*\rangle \quad \text{(A.8)}$$

$$\langle|F_{vv}|^2\rangle \cong (1-2\sigma_\phi^2)\langle|f_b|^2\rangle + 2\sigma_\phi^2\langle f_a f_b^*\rangle \quad \text{(A.9)}$$

where σ_ϕ is the standard deviation of the canting angle.

ACKNOWLEDGMENT

The authors would like to thank Prof. W. F. Krajewski and A. Kruger of Iowa State University, Ames, for making the video disdrometer data available. They would also like to thank J. S. Lutz and M. A. Randall for making the flawless performance of S-Pol possible, and radar operators D. A. Ferraro, A. D. Phiney, T. D. Rucker, M. A. Strong, and J. P. Vinson. In addition, they would like to thank R. A. Rilling and J. Hearst for preparing the radar tape for analysis, and R. Oye for software support.

REFERENCES

[1] T. A. Seliga and V. N. Bringi, "Potential use of radar differential reflectivity measurements at orthogonal polarizations for measuring precipitation," *J. Appl. Meteorol.*, vol. 15, pp. 69–76, 1976.

[2] H. N. Al-Khatib, T. A. Seliga, and V. N. Bringi, "Differential reflectivity and its use in the radar measurement of rain fall," Atmos. Sci. Prog. Rep. AS-S-106, The Ohio State Univ., Columbus, 1979.

[3] J. D. Doviak and D. S. Zrnic, *Doppler Radar and Weather Observations*, 2nd ed. San Diego, CA: Academic, 1993.

[4] J. Vivekanandan, D. S. Zrnic, S. M. Ellis, R. Oye, A. V. Ryzhkov, and J. Straka, "Cloud micro-physical retrieval using S-band dual-polarization radar measurements," *Bull. Amer. Meteorol. Soc.*, vol. 80, no. 3, pp. 381–388, 1999.

[5] A. Zahrai and D. S. Zrnic, "The 10 cm-wavelength polarimetric weather radar at NOAA's National Severe Storms Laboratory," *J. Atmos. Ocean. Technol.*, vol. 10, no. 5, pp. 649–661, 1993.

[6] V. N. Bringi and A. Hendry, "Technology of polarization diversity radars of meteorology," in *Radar in Meteorology*. Boston, MA: Amer. Meteorol. Soc., 1990, pp. 153–190.

[7] V. Chandrasekar and V. N. Bringi, "Error structure of multiparameter radar and surface measurements of rain—Part I: Different reflectivity," *J. Atmos. Ocean. Technol.*, vol. 5, pp. 783–795, 1988.

[8] ——, "Error structure of multiparameter radar and surface measurements of rain—Part II: X-band attenuation," *J. Atmos. Ocean. Technol.*, vol. 5, pp. 796–802, 1988.

[9] V. Chandrasekar, V. N. Bringi, N. Balakrishnan, and D. S. Zrnic, "Error structure of multiparameter radar and surface measurements of rain—Part III: Specific differential phase," *J. Atmos. Ocean. Technol.*, vol. 7, pp. 621–629, 1988.

[10] A. R. Jameson, "Relations among linear and circular polarization parameters measured in canted hydrometeors," *J. Atmos. Ocean. Technol.*, vol. 4, pp. 634–645, 1987.

[11] ——, "Microphysical interpretation of multiparameter radar measurements in rain—Part I: Interpretation of polarization measurements and estimation of raindrop shapes," *J. Atmos. Sci.*, vol. 40, pp. 1792–1802, 1983.

[12] ——, "Microphysical interpretation of multiparameter radar measurements in rain—Part II: Estimation of raindrop distribution parameters by combined dual-wavelength and polarization measurements," *J. Atmos. Sci.*, vol. 40, pp. 1803–1813, 1983.

[13] A. V. Ryzhkov, D. S. Zrnic, E. A. Brandes, J. Vivekanandan, V. N. Bringi, and G. Huang, "Characteristics of hydrometeor orientation obtained from radar polarimetric measurements in a linear polarization basis," in *Int. Geoscience and Remote Sensing Symp.*, Hamburg, Germany, June 28–July 2 1999.

[14] J. Vivekanandan, G. Zhang, and A. V. Ryzhkov, "Estimation of canting angle distribution of raindrop spectra using radar measurements," in *Bull. Int. Radar Symp.*, Calcutta, India, Dec. 1999.

[15] M. Sachidananda and D. S. Zrnic, "Rain rate estimates from differential polarization measurements," *J. Atmos. Ocean. Technol.*, vol. 4, pp. 588–598, 1987.

[16] C. W. Ulbrich and D. Atlas, "Rain microphysics and radar properties: Analysis methods for drop size spectra," *J. Appl. Meteorol.*, vol. 37, pp. 912–923, 1998.

[17] J. S. Marshall and W. Palmer, "The distribution of raindrops with size," *J. Meteorol.*, vol. 5, pp. 165–166, 1948.

[18] J. O. Law and D. A. Parson, "The relationship of raindrop size to intensity," *Trans. Amer. Geophys. Union*, vol. 24, pp. 452–460, 1943.

[19] C. W. Ulbrich, "Natural variations in the analytical form of the raindrop size distribution," *J. Climate Appl. Meteorol.*, vol. 22, pp. 1764–1775, 1983.

[20] T. Kozu and K. Nakamura, "Rain parameter estimation from dual-radar measurements combining reflectivity profile and path-integrated attenuation," *J. Atmos. Ocean. Technol.*, vol. 8, pp. 259–270, 1991.

[21] A. Tokay and D. A. Short, "Evidence for tropical raindrop spectra of the origin of rain from stratiform versus convective clouds," *J. Appl. Meteorol.*, vol. 35, pp. 355–371, 1996.

[22] A. W. Green, "An approximation for the shape of large raindrops," *J. Appl. Meteorol.*, vol. 14, pp. 1578–1583, 1975.

[23] Z. S. Haddad, S. L. Durden, and E. Im, "Parameterizing the raindrop size distribution," *J. Appl. Meteorol.*, vol. 35, pp. 3–13, 1996.

[24] Z. S. Haddad, D. A. Short, S. L. Durden, E. Im, S. Hensley, M. B. Grable, and R. A. Black, "A new parameterizing of raindrop size distribution," *IEEE Trans. Geosci. Remote Sensing*, vol. 35, pp. 532–539, May 1997.

[25] P. T. Willis, "Functional fits to some observed drop size distributions and parameterization of rain," *J. Atmos. Sci.*, vol. 41, no. 9, pp. 1648–1661, 1984.

[26] A. J. Illingworth and T. M. Blackman, "Normalized gamma functions for raindrop size distribution and the interpretation of polarization radar observations," J. Appl. Meteorol., March 1998, submitted for publication.

[27] P. S. Ray, "Broadband complex refractive indices of ice and water," *Appl. Opt.*, vol. 11, pp. 1836–1844, 1972.

[28] V. N. Bringi, "Raindrop size distribution," private communication, 1999.

[29] H. Sauvageot and J. Lacaux, "The shape of averaged drop size distributions," *J. Atmos. Sci.*, vol. 52, no. 8, pp. 1070–1083, 1995.

[30] C. Richter and M. Hagen, "Drop-size distributions of raindrops by polarization radar and simultaneous measurements with disdrometer, windprofiler, and PMS probes," *Q. J. R. Meteorol. Soc.*, vol. 122, pp. 2277–2296, 1997.

[31] V. N. Bringi, V. Chandrasekar, and R. Xiao, "Raindrop axis ratios and size distributions in Florida rainshafts: An assessment of multiparameter radar algorithms," *IEEE Trans. Geosci. Remote Sensing*, vol. 36, pp. 703–715, May 1998.

[32] V. N. Bringi and V. Chandrasekar, Polarimetric Doppler Weather Radar-Principle and Application. New York: Oxford, 2000, to be published.

[33] D. S. Zrnic, T. D. Keenan, and L. D. Carey, "Sensitivity analysis of polarimetric variables at a 5-cm wavelength in rain," J. Appl. Meteorol., 1999, submitted for publication.

[34] M. Schonhuber, H. E. Urban, J. P. V. P. Baptista, W. L. Randeu, and W. Riedler, "Weather radar versus 2D-video disdrometer data," in *Weather Radar Technology for Water Resources Management*, B. Braga Jr. and O. Massambani, Eds. Montevideo, Uruguay: UNESCO, 1997, pp. 159–171.

[35] A. R. Holt, "Some factors affecting the remote sensing of rain by polarization diversity radar in the 3 to 35 GHz frequency range," *Radio Sci.*, vol. 19, pp. 1399–1412, 1984.

Guifu Zhang received the B.S. degree in physics from Anhui University, in 1982, the M.S. degree in radio physics from Wuhan University, Wuhan, China, in 1985, and the Ph.D. degree in electrical engineering from the University of Washington, Seattle, in 1998.

From 1985 to 1993, he was with the Space Physics Department, Wuhan University, as an Assistant Professor and Associate Professor. In 1989, he was a Visiting Scholar working at the Communication Research Laboratory, Japan. From 1993 to 1998, he studied and worked in the Department of Electrical Engineering, University of Washington, where he first was a Visiting Scientist and later a Ph.D. student. He is currently a Project Scientist with the National Center for Atmospheric Research. His research interests include modeling of wave propagation and scattering in random media and from rough surface, development of remote sensing techniques for environmental monitoring, and target detection.

J. Vivekanandan received the B.E. degree in electronics and communications engineering from Madurai-Kamaraj University, the M.Tech. degree in microwave and radar engineering from the Indian Institute of Technology, Kharagpur, India, and the Ph.D. degree in electrical engineering from Colorado State University, Fort Collins, in 1986.

Currently he is a Scientist with the National Center for Atmospheric Research, Boulder, CO. His research experience includes microwave radar and radiometer/satellite remote sensing of the atmosphere, vegetation, and soil. He has devoted considerable effort toward modeling polarimetric radar and multifrequency radiometer observations in clouds and their interpretations. He has participated in a number of field programs that involved radar, aircraft, satellite, and ground-based instruments.

Edward Brandes received the B.S. degree in mechanical engineering from the New Jersey Institute of Technology, Newark, the M.S. degree in meteorology from New York University, and the Ph.D. degree in meteorology from the University of Oklahoma, Norman.

From 1970 to 1991, he was a Research Meteorologist with the National Severe Storms Laboratory, Norman. Since 1991, he has been with at the National Center for Atmospheric Research, Boulder, CO. His research interests are in meteorological applications of polarimetric radar, with emphasis on rainfall estimation and weather hazard detection.